Electronic Supplementary Material (ESI) for ChemComm.

Electronic supplementary information

Non-thermal Plasma Induced Photocatalytic Conversion of Light Alkanes into High Value-added Liquid Chemicals at Near Ambient Conditions

Aiguo Wang [a], Shijun Meng [a], Hua Song *[a]

[a] Department of Chemical and Petroleum Engineering, University of Calgary, 2500 University Dr NW, Calgary, Alberta T2N 1N4, Canada

*Corresponding author

Fax: +1 (403) 284-4852; Tel: +1 (403) 220-3792;

E-mail: sonh@ucalgary.ca

Experimental

Catalyst preparation

The ammonium ZSM-5 zeolite powder with SiO_2/Al_2O_3 molar ratio of 80 (Zeolyst CBV 8014) were calcined at 600 ℃ for 5 h in air to obtain HZSM-5 powder. UZSM-5 (Uniform Zeolite Socony Mobil-5) support was prepared by hydrothermal synthesis. $Al(NO_3)_3 \cdot 9H_2O$ (98%, Alfa Aesar) as the alumina precursor was dissolved in tetrapropylammonium hydroxide (TPAOH, 1.0 M, Sigma-Aldrich) stirred at room temperature until a clear solution was obtained. The initial hydrolysis of tetraethyl orthosilicate (TEOS) as silica source was achieved by adding dropwise TEOS to the above solution. The molar ratio of Al_2O_3: SiO_2: TPAOH: H_2O was 1: 80: 21: 943. The solution kept stirring at room temperature until the gel was obtained. The resulting supersaturated solution was transferred in an autoclave and held at 170 °C for 3 days. After cooling down to room temperature, the solid was recovered by centrifuge, washed with deionized water and dried at 110 °C for 12 h, ramped at 5 °C/min to 300 °C for 1 h, then calcined in air at 600 °C for 6 h. The synthesized powder was named as UZSM-5. The powder (HZSM-5, UZSM-5) was then extruded and calcined at 600 ºC for 5 h in air. The extruded sample was manually cut into pellets with a diameter of 2 mm and 5-10 mm length. SiO_2 (Alfa Aesar, 160 $m^2 \cdot g^{-1}$) is commercially available and purchased from Alfa Aesar.

The catalysts Ga/UZSM-5 and Pt/UZSM-5 were prepared via wet impregnation (WI) using $Ga(NO_3)_3 \cdot xH_2O$ (99.9%, Sigma-Aldrich) and $Pt(NH_3)_4(NO_3)_2$ (≥50.0% Pt basis, Sigma-Aldrich) as the precursor, respectively. WI was made by initially dissolving the corresponding amount (1wt.%) of the precursor in 60.0 g deionized water, then 8.0 g pelleted UZSM-5 was dispersed in the precursor solution and kept rotating (100 rpm) for

2 hours at 60 ºC on rotary evaporator. Water was then completely evaporated at 60 ºC and the resulting catalyst was dried in the oven at 110 ºC overnight, followed by calcination at 550 ºC with a heating rate of 5 °C/min and a holding time of 3 h in ambient air.

The catalyst Ti/UZSM-5 was prepared by chemical vapor deposition described by Zhang. [1] 6.0 g pelleted UZSM-5 was put into the quartz reactor and dehydrated in the dry nitrogen at 473 K for 3 h. Then the temperature was set to 873 K. when the temperature stabilized, chemical vapor deposition was initiated by switching Tetrabutyltitanate (Sigma-Aldrich, 97%, TBOT) as Ti precursor with a carrier gas flow rate of 200 ml/min and the precursor temperature was 333 K. TBOT was transported into the reactor where it decomposed and TiO_2 particles formed. After 3 h of deposition at 873 K, the reactor was purged by nitrogen gas for 1 h. The Ti-Ga/UZSM-5 was prepared by chemical vapor deposition described above using pelleted Ga/UZSM-5 as the starting material.

Plasma induced photocatalytic conversion of light alkanes

The plasma catalytic conversion of light alkanes was carried out in a coaxial dielectric barrier discharge (DBD) reactor at room temperature and atmospheric pressure. The details of the apparatus could be found in our previous work. [2] In a typical run, 6.0 g pelleted catalyst was packed in DBD reactor, and then a mixture of C_3H_8 (99.5%, Praxair), *n*-C_4H_{10} (99.5%, Praxair) with Ar (99.999%, Praxair) were introduced into the reactor. Ar is used as the balanced gas because Ar can facilitate the plasma generation without participation into the reaction. The flow rates of C_3H_8, *n*-C_4H_{10} and Ar were controlled by mass flow controllers and set to be 5, 5, and 40 sccm, respectively. All the experiments were conducted at ca. 9.25 kV peak to peak at load with a constant frequency of 17 kHz

at room temperature with 40 min of reaction time. The plasma discharge power was 24-27 W. After reaction, the temperature of the discharge zone was around 200 ºC. In the catalyst only mode, the reaction was performed at a temperature of around 200 ºC.

The gas products were analyzed by a four-channel micro-GC (Agilent 490) equipped with a thermal conductivity detector. The first channel equipped with a 10 m molecular sieve 5A column, which can accurately analyze H_2, O_2, CH_4, and CO. CO_2, C_2H_2, C_2H_4, and C_2H_6 are analyzed in the second channel with a 10 m PPU column. C_3-C_6 and $C_{3=}$-$C_{6=}$ hydrocarbons are determined in the third and fourth channels charged with a 10 m alumina column and an 8 m CP-Sil 5 CB column, respectively. Ar is the carrier gases for the first channel, and He is used as the carrier gas for the other three channels. The composition of gas products determined by micro-GC was used to calculate the conversion of light alkanes as well as the yield of gas products based on the ideal gas law. The gas flow rate before and after the reaction was measured using a soap-film flowmeter.

A chiller (-15 ºC) was used to cool the condenser and trap the liquid products. 10 ml of carbon disulfide (99.9%, Sigma-Aldrich) was added to wash the liquid products out from the condenser and reactor, and then used to extract the liquid products on the catalyst. The composition of liquid products was analyzed by the pre-calibrated Gas Chromatography-Mass Spectrometer (GC–MS: PerkinElmer GC Claus 680 and MS Clarus SQ 8T) equipped with a Paraffins-Olefins-Naphthenes-Aromatics (PONA) column (Agilent HP-PONA). The oven temperature of GC was set to hold at 40 ºC for 1 min, rise to 110 ºC at 5 ºC /min, ramp to 200 ºC at 10 ºC /min and hold for 5 min. A split ratio of 20 was used for the GC-MS analysis. The mass detector was set to scan the m/z range from

10 to 400. Identification of the compounds was achieved by comparing the mass spectra obtained with those in the system's database (NIST).

The conversion of light hydrocarbon (C_nH_{2n+2}, n=1, 2, 3, 4) was calculated by:

$$C_nH_{2n+2}\ \text{conversion}\ (\%) = \frac{\text{moles of } C_nH_{2n+2} \text{ converted}}{\text{moles of } C_nH_{2n+2} \text{ fed}} \times 100$$

The yield of hydrocarbons (C_i) in gas products (Y_i) was given by:

$$Y_i\ (C\ \%) = \frac{i \times \text{moles of } C_i \text{ produced}}{\sum_{n=1}^{4} n \times \text{moles of } C_nH_{2n+2} \text{ converted}} \times 100\ (i = 1, 2, 3, 4, 5)$$

The yield of total gas products (Y_G, C %) was calculated by:

$$Y_G(C\ \%) = \sum_{i=1}^{5} Y_i$$

The coke yield (Y_C, C %) was determined by TGA profiles, in which the coke was calculated by weight loss from 300 to 700 °C assuming coke is composed of pure carbon.

The yield of liquid product (Y_L, C %) was defined as: $Y_L(C\ \%) = 100 - Y_G - Y_C$

Characterizations

Pyridine absorption: DRIFT spectrum upon pyridine absorption was acquired with a Thermo-Scientific-Nicolet iS50 equipped with an environmental chamber and a liquid-nitrogen cooled mercury–cadmium–telluride (MCT) detector. The gas inlet was connected to a bubbler for pyridine introduction via two three-way valves. Inlet gas (N_2) could pass through the pyridine before entering the chamber. For pyridine adsorption, the fresh catalyst was loaded in the environmental chamber with a 30 sccm N_2 flow for 30 min before collecting background spectra at room temperature (25 ºC). The N_2 flow was

then sent into the bubbler and carried pyridine vapor into the environmental chamber to conduct pyridine absorption for 20 min. After that, N_2 flow was switched back to bypass the bubbler. The spectrum was recorded in an absorbance mode upon stabilization for 20 min at room temperature.

NH_3-TPD: NH_3-TPD experiments were conducted on the Finesorb-3010 Chemisorption Analyzer. Ammonia was selected as a probe due to its simplicity, small molecular size, and ability to titrate both strong and weak acid sites on the catalyst. Prior to measurements, ~250 mg of fresh sample was calcinated in He flow with 30 sccm at 600 °C for 30 min with a ramp rate of 20 °C/min. The sample was then cooled to 120 °C for adsorption of ammonia using a flow of 25 sccm of 10% NH_3/He for 30 min. After flowing He for 10 min to remove any physically adsorbed NH_3 at 120 ºC, TPD was carried out by ramping to 600 °C with at 10 °C/min and a hold of 30 min under He with the flow rate of 25 sccm. A thermal conductivity detector (TCD) determined the amount of desorbed NH_3. The acquired profiles were fitted and deconvoluted using Bigaussian.

XRD: The powder X-ray Diffraction (XRD) analysis of the catalysts was carried out on a Rigaku ULTIMA III X-ray diffractometer with a Cu Kα irradiation source at a voltage of 40 kV and current of 44 mA. All powder diffraction data were acquired between a 2θ of 3-60º, using 2º step/min.

TGA: Thermographic Analysis (TGA) profiles were used to determine the coke formation and acquired with a simultaneous thermal analyzer (PerkinElmer STA 6000). The samples were held at 30 ºC for 1 min, then heated to 800 ºC at a rate of 20 ºC/min under 30 mL/min air flow.

GC-MS analysis

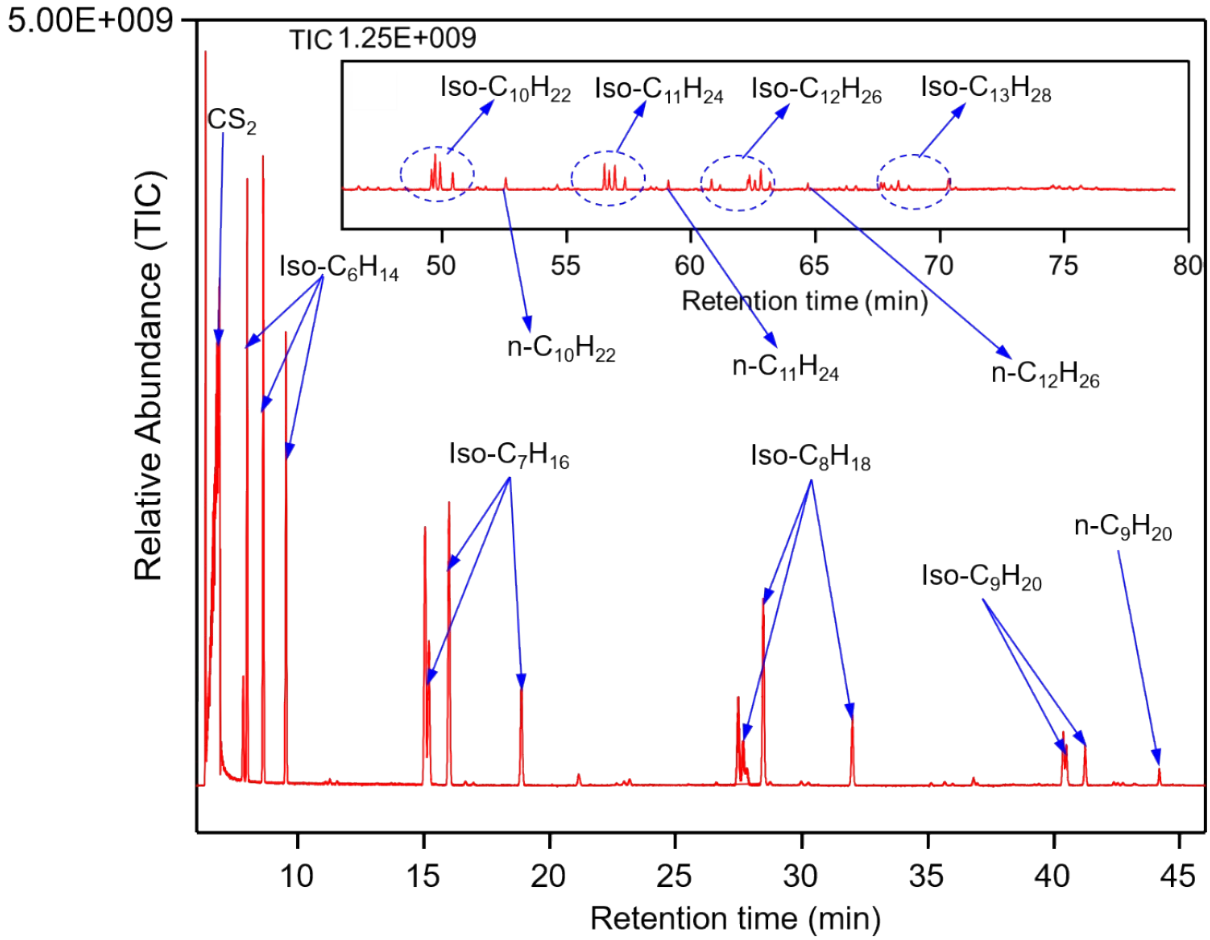

Figure S1. The total ion chromatogram (TIC) of liquid products collected from the plasma catalytic conversion of propane and butane over HZSM-5 and structures of identified compounds. (the products were collected through extraction using CS_2 as the solvent).

Table S1. Possible reactions in the conversion of propane and butane under plasma conditions

No.	Elementary reaction	Rate constant	Ea, kJ/mol
R1	$C_3H_8 \rightarrow \cdot C_2H_5 + \cdot CH_3$	1.47E-48	383
R2	$C_3H_8 \rightarrow n\text{-}C_3H_7\cdot + H\cdot$	1.32E-55	408

R3	$C_3H_8 \rightarrow (CH_3)_2CH\cdot + H\cdot$	5.59E-54	397
R4	$n\text{-}C_3H_7\cdot \rightarrow C_2H_4 + \cdot CH_3$	3.75E-10	129
R5	$n\text{-}C_4H_{10} \rightarrow n\text{-}C_3H_7\cdot + \cdot CH_3$	2.14E-45	354
R6	$n\text{-}C_4H_{10} \rightarrow \cdot C_2H_5 + \cdot C_2H_5$	2.60E-42	336
R7	$n\text{-}C_4H_{10} \rightarrow n\text{-}C_4H_9\cdot + H\cdot$	6.75E-56	410
R8	$n\text{-}C_4H_{10} \rightarrow C_2H_5(CH_3)CH\cdot + H\cdot$	6.34E-54	397
R9	$n\text{-}C_4H_9\cdot \rightarrow C_2H_4 + \cdot C_2H_5$	1.65E-8	123
R10	$H\cdot + H\cdot \rightarrow H_2$	1.21E-32	-1.51
R11	$\cdot CH_3 + H\cdot \rightarrow CH_4$	2.29E-10	1.67
R12	$\cdot CH_3 + \cdot CH_3 \rightarrow C_2H_6$	6.00E-11	2.45
R13	$\cdot C_2H_5 + H\cdot \rightarrow C_2H_6$	2.25E-10	-
R14	$\cdot C_2H_5 + \cdot CH_3 \rightarrow C_3H_8$	8.22E-11	-2.15
R15	$(CH_3)_2CH\cdot + \cdot CH_3 \rightarrow iso\text{-}C_4H_{10}$	4.94E-11	-0.81
R16	$n\text{-}C_3H_7\cdot + \cdot CH_3 \rightarrow n\text{-}C_4H_{10}$	5.15E-11	-
R17	$\cdot C_2H_5 + \cdot C_2H_5 \rightarrow n\text{-}C_4H_{10}$	2.71E-11	-0.01
R18	$(CH_3)_2CH\cdot + \cdot C_2H_5 \rightarrow C_5H_{12}$	3.07E-11	-1.34
R19	$\cdot CH_3 + C_2H_5(CH_3)CH\cdot \rightarrow C_5H_{12}$	5.15E-11	-
R20	$(CH_3)_2CH\cdot + n\text{-}C_3H_7\cdot \rightarrow (CH_3)_2CH(CH_2)_2CH_3$	2.90E-11	-
R21	$(CH_3)_2CH\cdot + (CH_3)_2CH\cdot \rightarrow (CH_3)_2CHCH(CH_3)_2$	1.11E-11	-1.1
R22	$(CH_3)_2CH\cdot + iso\text{-}C_4H_9\cdot \rightarrow (CH_3)_2CHCH_2CH(CH_3)_2$	2.90E-11	-
R23	$C_2H_5(CH_3)CH\cdot + n\text{-}C_3H_7\cdot \rightarrow CH_3(CH_2)_2CH(CH_3)CH_2CH_3$	1.59E-11	-
R24	$C_2H_5(CH_3)CH\cdot + (CH_3)_2CH\cdot \rightarrow (CH_3)_2CHCH(CH_3)CH_2CH_3$	1.52E-11	-0.54
R25	$iso\text{-}C_4H_9\cdot + iso\text{-}C_4H_9\cdot \rightarrow (CH_3)_2CHCH_2CH_2CH(CH_3)_2$	1.66E-10	-
R26	$C_2H_5(CH_3)CH\cdot + C_2H_5(CH_3)CH\cdot \rightarrow CH_3CH_2CH(CH_3)CH(CH_3)C_2H_5$	6.06E-1	2.09

Reaction conditions for determining the rate constant: 1 atm, 298-300 K; Units of rate constant: $cm^3\ mol^{-1}\ s^{-1}$ for bimolecular; $cm^6\ mol^{-2}\ s^{-1}$ for termolecular reaction. The rate constant is calculated from the Arrhenius expression. [3]

Table S2. The effect of operating mode on the conversion of propane and butane

Operating mode		Catalyst only	Plasma only	Plasma + catalyst
Conv. (%)	C_3H_8	0.0	29.7	33.3
	n-C_4H_{10}	0.0	9.2	10.1
		The yield of products (C %)		
Gas	CH_4	0.0	16.6	9.6
	C_2H_6, C_2H_4	0.0	52.3	32.9
	n-C_5H_{12}	0.0	4.1	4.2
	Sum	0.0	73	46.7
Liquid		0.0	6.4	47.8
Coke		0.0	20.6	5.5
		The composition of liquid product (C %)		
C_6		N/A	N/A	40.2
C_7		N/A	N/A	37.5
C_8		N/A	N/A	18.1
C_9		N/A	N/A	4.2
≥C_{10}		N/A	N/A	0.0

Reaction conditions: 50 sccm of gas mixture (10% C_3H_8, 10% *n*-C_4H_{10}, 80% Ar), 40 min, discharge power 24-27 W, catalyst *ca.* 6 g. The catalyst used in “catalyst only” and “plasma + catalyst” mode is Ti-Ga/UZSM-5. There is no catalyst in “plasma only” mode.

Table S3. Non-thermal plasma catalytic conversion of different light alkanes to liquid chemicals

Light alkanes	CH_4	C_2H_6	C_3H_8	n-C_4H_{10}	CH_4 + C_3H_8		C_3H_8 + *n*-C_4H_{10}	
Conversion (%)	23.7	26.9	27.1	25.9	CH_4	3.3	C_3H_8	33.3
					C_3H_8	36.4	n-C_4H_{10}	10.1
	The yield of products (C %)							
C_1	0.0	8.6	10.0	7.4	0.0		9.6	
C_2	51.9	18.1	38.0	36.5	25.9		32.9	
C_3	17.1	9.8	1.0	8.4	13.7		0.0	
C_4	4.8	16	7.2	0.0	8.4		0.0	
C_5	1.4	3.2	5.1	5.5	3.2		4.2	
C_6-C_9	3.5	15.8	30.5	36.9	43.4		47.8	
Coke	21.2	28.5	8.1	7.3	5.3		5.5	
Selectivity of C-C coupling reaction	78.7	44.8	42.9	42.4	55.0		52.0	

Reaction conditions: 40 min, discharge power 24-27 W, *ca.* 6 g catalyst Ti-Ga/UZSM-5, 50 sccm of gas mixture; for a pure alkane C_nH_{2n+2} (n=1, 2, 3, 4), the composition of gas mixture is 20 % of C_nH_{2n+2} and 80 % Ar; for the mixture of CH_4+C_3H_8, the composition of gas mixture is 10% CH_4, 10% C_3H_8, and 80% Ar; for the mixture of C_3H_8 + *n*-C_4H_{10}, the composition of gas mixture is 10% C_3H_8, 10% *n*-C_4H_{10}, and 80% Ar. The selectivity of C-C coupling reaction for light hydrocarbon C_nH_{2n+2} is defined as the total yield of C_{n+1}-C_9 hydrocarbon (n=1, 2, 3, 4; for the mixture of CH_4+C_3H_8 or C_3H_8+*n*-C_4H_{10}, n=3 or 4, respectively).

DRIFT (Diffuse-Reflectance FTIR)

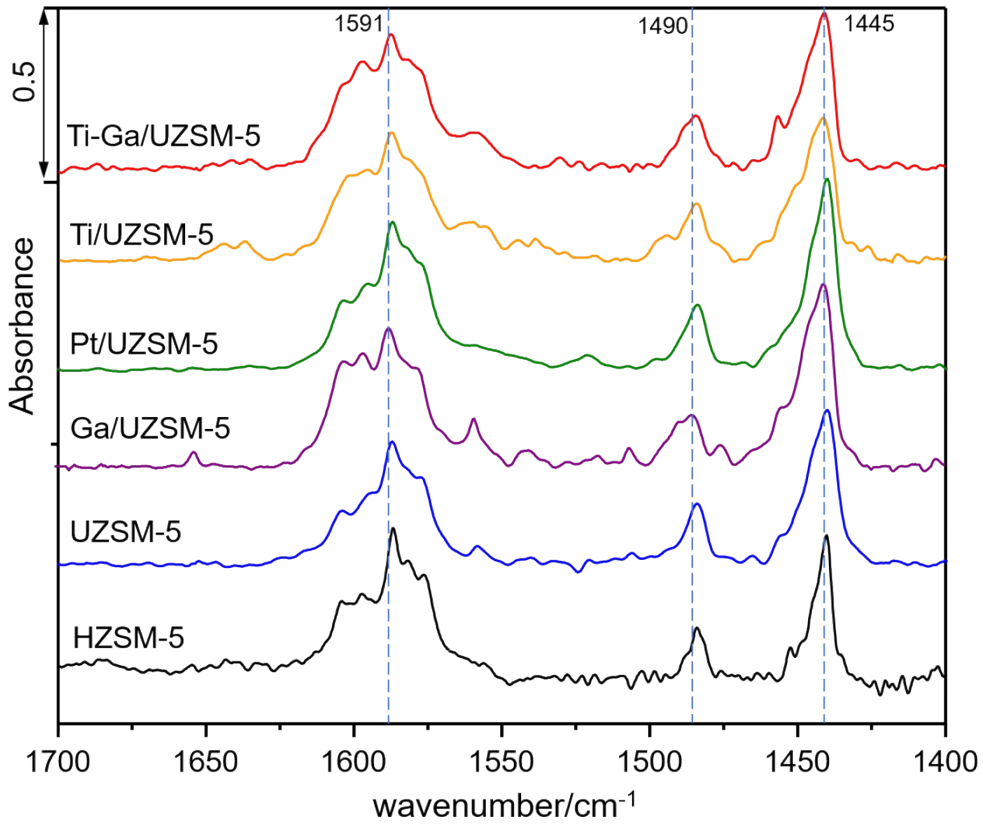

Figure S2. DRIFT spectra collected over various fresh catalysts upon pyridine adsorption

The peaks around 1445 cm^{-1} are assigned to Lewis acid sites. The peaks at 1490 cm^{-1} are assigned to coordinately bonded pyridine (pyridine and pyridinium ion) due to the Lewis acid sites and Bronsted acid sites. The broad peaks around 1590 cm^{-1} are assigned to the hydrogen-bonded pyridine closely associated to Bronsted acid sites.[4-7] Spectra of all catalysts have the typical signals for pyridine molecules protonated at Bronsted sites and pyridine coordinated at Lewis sites with the similar distribution, which implies that the characteristic of Bronsted and Lewis acidic sites is not determining factors for the reaction performance.

NH_3-TPD

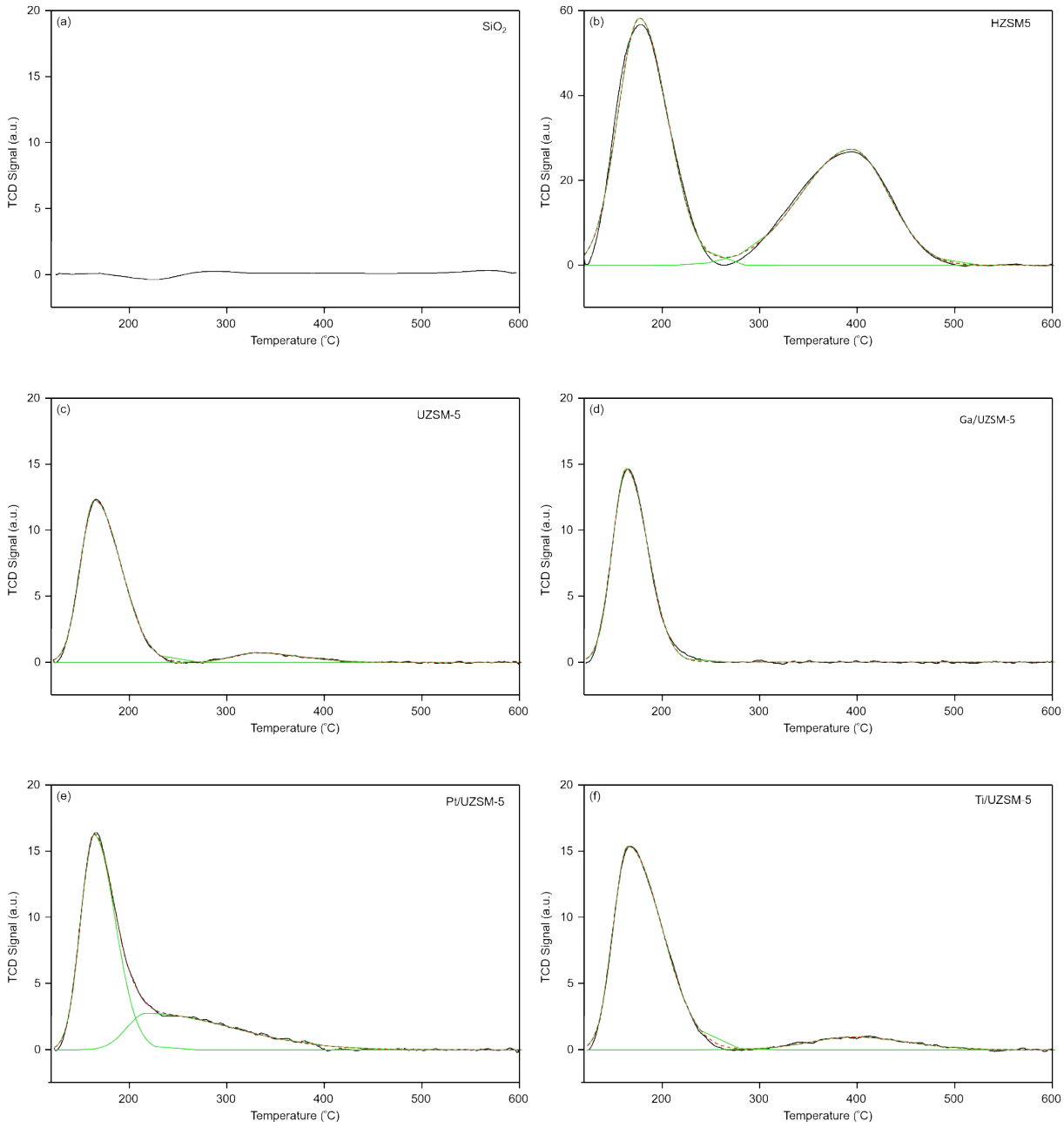
(a)
SiO2
(b)
HZSM5
(c)
UZSM-5
(d)
Ga/UZSM-5
(e)
Pt/UZSM-5
(f)
Ti/UZSM-5
TCD Signal (a.u.)
Temperature (℃)

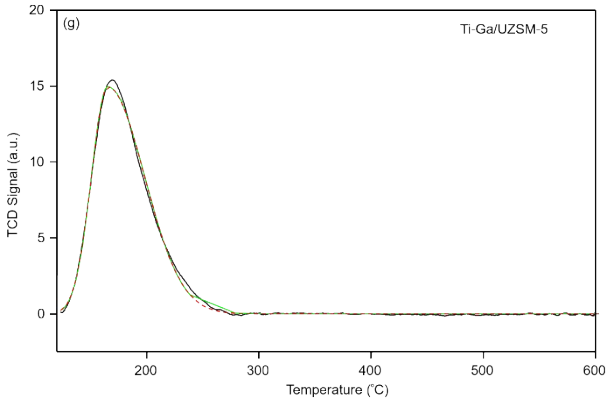

Figure S3. NH_3-TPD profiles and Bigaussian deconvoluted peaks of various fresh catalysts, (a) SiO_2, (b) HZSM-5, (c) UZSM-5, (d) Ga/UZSM-5, (e) Pt/UZSM-5, (f) Ti/UZSM-5, (g) Ti-Ga/UZSM-5. Black solid line is the experimental data, red dash line is the fitting data, and green solid line is the deconvoluted peak.

The acid sites over the catalysts have distinctive acidic properties as shown in NH_3-TPD profiles in **Table 2** and **Figure S3.** The peaks in the low temperature region (< 200 ºC) originate from NH_3 molecules desorbed from the weak acidic sites, and the peaks located in the range of 200-400 ºC is indicative of the presence of sites with medium acidity [8], while the peaks at high temperature (> 400 ºC) is probably associated with NH_3 molecules desorption from strong surface acidic sites. [9, 10] It is obvious that the formation of liquid products is significantly influenced by the distribution of weak, medium and strong acidic sites over the catalyst. Severe coke and limited liquid products are observed over the catalyst with no acidic sites (SiO_2) or a high ratio of strong acidic sites (46%, HZSM-5), while a high yield of liquid products with limited coke formation is achieved over UZSM-5 with a high ratio of weak acidic sites (91%). Compare to UZSM-5, Ga addition completely removes medium acidic sites of UZSM-5 and the similar phenomenon is observed when co-loading of Ti and Ga on UZSM-5. Plasma reactions with Ga/UZSM-5 (entry 4) or Ti-Ga/UZSM-5 (entry 7) produce more liquid products with less coke formation. However, the liquid yield (47.8 C%) over Ti-Ga/UZSM-5 is higher than that (39.8 C%) over Ga/UZSM-5 as a result of the synergy between Ti and Ga. Pt loading deceases the ratio of weak acidic sites by introducing more medium acidic sites, thus increasing the gas yield by 6.3 C%. The adding of Ti on UZSM-5 leads to a slight drop in

the ratio of weak acidic sites with the appearance of the strong acidic sites, which produces severe coke formation with more gas products. These observations suggest that the catalyst with a higher ratio of weak acidic sites favors the formation of liquid products with less coke. The presence of acidic sites enhances the stabilization of the reactive radicals and promotes the recombination of highly reactive species to form liquid products via a Langmuir-Hinshelwood mechanism. [11] The weak interaction between weak acidic sites and radicals allows the formed products to be desorbed from the catalyst surface readily and leave the plasma zone or migrate inside the catalyst pores without the excessive electron-impact dissociation. While the strong bonding between strong/medium acidic sites and reactive species would trap the products on the surface, which are further dissociated to be coke and gas products because of the constant attack by highly energetic electrons.

XRD

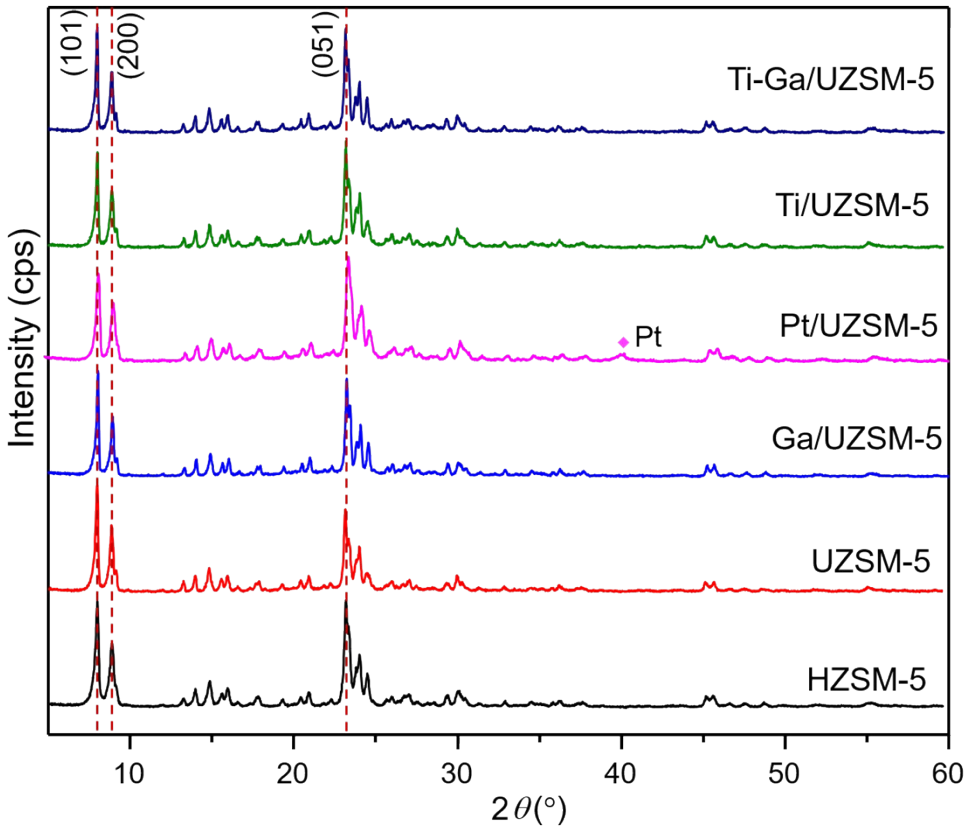

Figure S4. Powder XRD patterns of various fresh catalysts

Powder XRD patterns of various fresh catalysts are shown in **Figure S4**. As expected, XRD patterns of UZSM-5 catalyst prepared by hydrothermal synthesis method shows a typical pattern of MFI structure ($2\theta \approx 8.0°$, 8.8°, and 23.3° corresponding to (101), (200), and (051) crystal planes), which are in good agreement with JCPDS No. 44-0005. The typical pattern of MFI structure is clearly detected on metal modified UZSM-5 catalysts. There is no additional peak appearing in the XRD patterns of these catalysts, suggesting that metal loading causes insignificant distortion of zeolite framework and the loaded metal species are well dispersed over the catalyst. The small diffraction peak at $2\theta = 40°$ on Pt/UZSM-5 catalyst is originated from Pt species (platinum oxide and platinum) due to the high absorption coefficient of Pt for XRD. [12] The crystallite size is estimated using Scherrer formula to (101), (200), and (051) reflections of PXRD patterns. The average crystallite sizes of UZSM-5 and HZSM-5 are calculated to be 30.2±0.3 nm and 38.9±0.4nm, respectively. Therefore, the change in the crystallite size may contribute to the differences in particle size/morphology as seen from SEM in Figure S5.

SEM

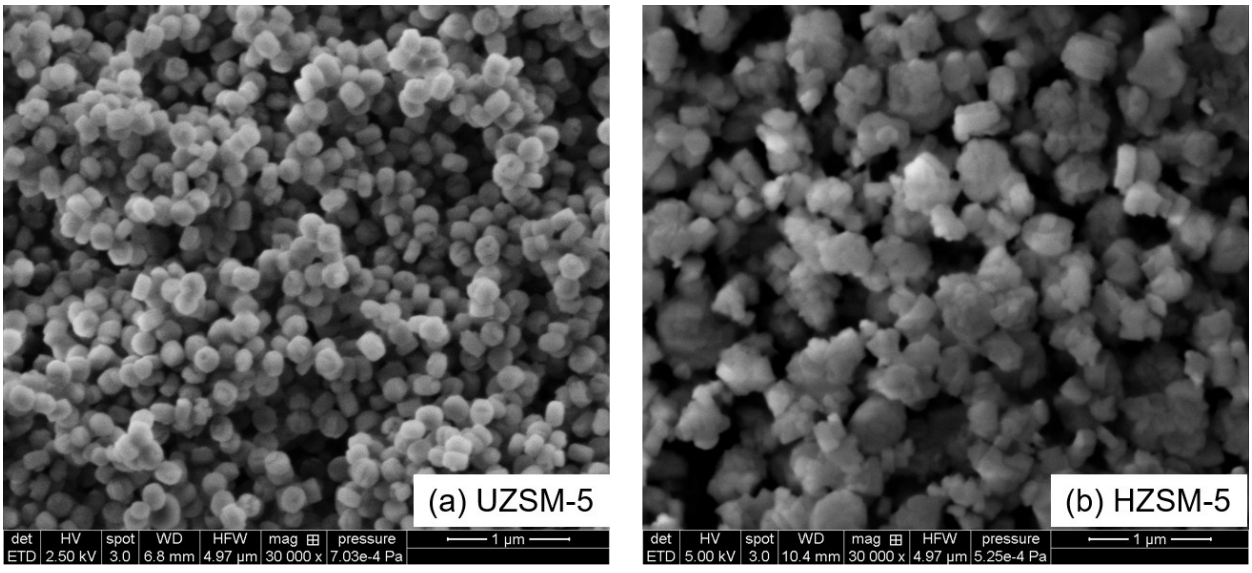

Figure S5. Scanning electron microscopy (SEM) images of the samples: (a) UZSM-5, (b) HZSM-5. SEM was performed on FEI XL30 in backscattered electron mode.

TGA

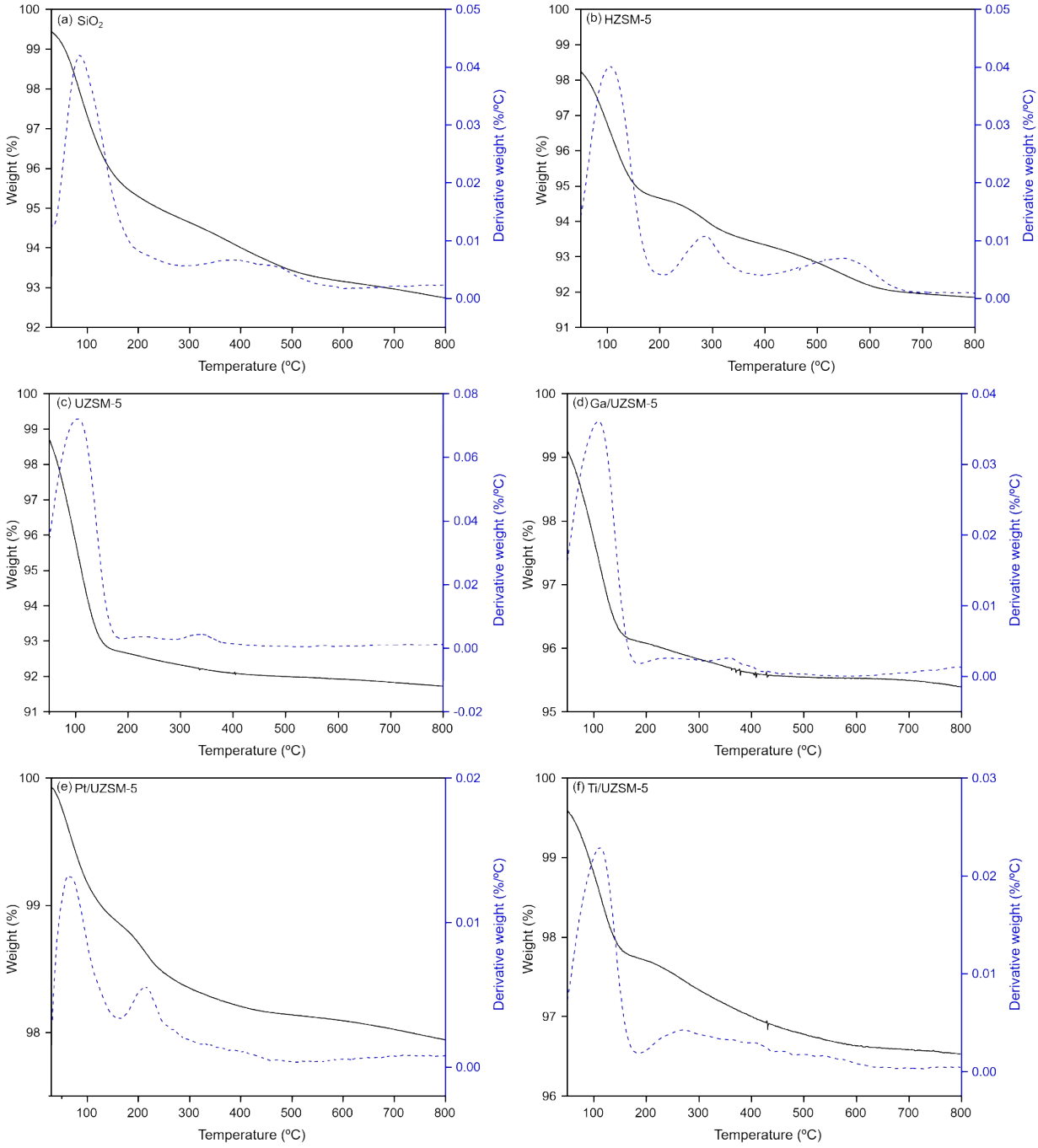
(a) SiO2
(b) HZSM-5
(c) UZSM-5
(d) Ga/UZSM-5
(e) Pt/UZSM-5
(f) Ti/UZSM-5
Weight (%)
Derivative weight (%/°C)
Temperature (°C)

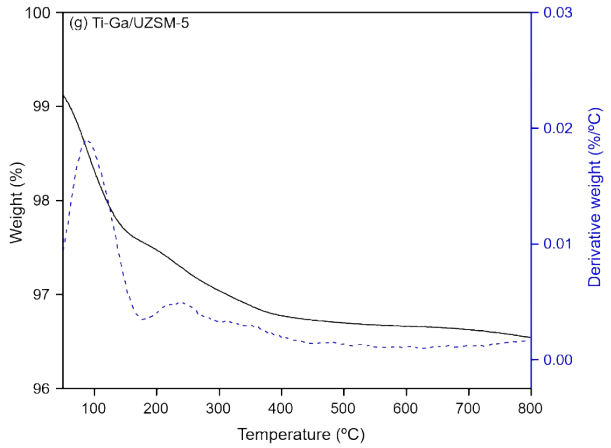

Figure S6. TGA profiles of the spent catalysts: (a) SiO_2, (b) HZSM-5, (c) UZSM-5, (d) Ga/UZSM-5, (e) Pt/UZSM-5, (f) Ti/UZSM-5, (g) Ti-Ga/UZSM-5.

Coke characterization by TGA in **Figure S6** shows that the active carbonaceous species in the form of amorphous carbon [13] (300-400 ºC) is formed on UZSM-5, Ga/UZSM-5, Pt/UZSM-5, and Ti-Ga/UZSM-5 after plasma reactions, while less active carbon deposition in the mixed form of amorphous and filamentous carbon [13] (400-600 ºC) is observed on SiO_2, HZSM-5, and Ti/UZSM-5.

Reference

1. X. Zhang, M. Zhou and L. Lei, *Applied Catalysis A: General*, 2005, **282**, 285-293.
2. A. G. Wang, J. H. Harrhy, S. J. Meng, P. He, L. J. Liu and H. Song, *Energy Conversion and Management*, 2019, **191**, 93-101.
3. W. G. Mallard, Westley, F., Herron, J.T., Hampson, R.,, *Chemical Kinetics Database: Version 2Q98.* , National Institute of Standards and Technology (NIST), 1998.
4. E. P. PARRY, *JOURNAL OF CATALYSIS* 1963, **2**, 371-379
5. D. Topaloğlu Yazıcı and C. Bilgiç, *Surface and Interface Analysis*, 2010, **42**, 959-962.
6. O. M. Busch, W. Brijoux, S. Thomson and F. Schüth, *Journal of Catalysis*, 2004, **222**, 174-179.
7. F. Hemmann, C. Jaeger and E. Kemnitz, *RSC Adv.*, 2014, **4**, 56900-56909.
8. H. Dong, L. Zhang, Z. Fang, W. Fu, T. Tang, Y. Feng and T. Tang, *RSC Advances*, 2017, **7**, 22008-22016.
9. J. V. Ferenc Lonyi, *Microporous and Mesoporous Materials*, 2001, **47**, 293-301.
10. Y. Cheng, Q. Zhao, Y. Li, W. Peng, G. Zhang, F. Zhang and X. Fan, *RSC Advances*, 2016, **6**, 76151-76157.
11. S. Kameshima, K. Tamura, Y. Ishibashi and T. Nozaki, *Catalysis Today*, 2015, **256**, 67-75.
12. M. Sun, S. Wang, Y. Li, Q. Wang, H. Xu and Y. Chen, *Journal of the Taiwan Institute of Chemical Engineers*, 2017, **78**, 401-408.
13. Y. X. Zeng, L. Wang, C. F. Wu, J. Q. Wang, B. X. Shen and X. Tu, *Applied Catalysis B: Environmental*, 2018, **224**, 469-478.